analytical chemistry

pubs.acs.org/ac Article

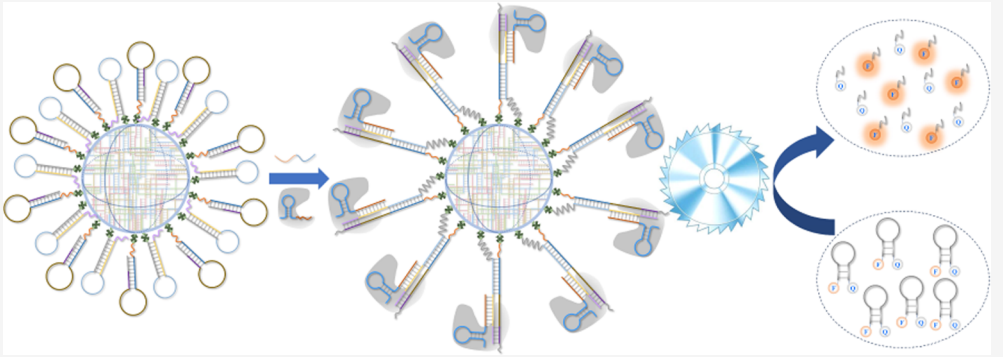
Dual-Accelerated Signal Amplification in Biosensing via Spatial Confining Catalytic Hairpin Assembly-Activated Spherical CRISPR/Cas12a System for Trans-Cleavage of Hairpin DNA Reporters

Zhuqi Sui, Baoqiang Chen, Jia Zhao, Haidong Yang, Longhua Guo, and Jianguo Xu*

Cite This: https://doi.org/10.1021/acs.analchem.4c07111 Read Online

ACCESS | Metrics & More | Article Recommendations | Supporting Information

Downloaded via SHANGHAI NORMAL UNIV on February 23, 2025 at 00:42:40 (UTC).
See https://pubs.acs.org/sharingguidelines for options on how to legitimately share published articles.



ABSTRACT: MicroRNAs (miRNAs) are small noncoding RNAs that regulate gene expression and are implicated in various diseases, including cancer. Due to their critical role in diagnostics, there is a growing need for sensitive, specific, and rapid detection methods for miRNAs. In this study, we present a dual-accelerated signal amplification platform for miRNA biosensing, which integrates spatial confining catalytic hairpin assembly (SC-CHA) with spherical CRISPR/Cas12a (S-CRISPR/Cas12a) system for (SC-CHA@S-CRISPR/Cas12a) trans-cleavage of hairpin DNA reporters. The method employs a biotinylated palindrome-rich assembly sequence (PAS) to form DNA nanoballs, which serve as a scaffold for the operation of SC-CHA upon miRNA binding. The SC-CHA products bind with crRNA and Cas 12a protein, activating S-CRISPR/Cas12a system to cleave the hairpin DNA reporter and generate a detectable fluorescence signal. The uniqueness of this system lies in the combined use of DNA nanoballs and hairpin DNA reporters, both of which significantly accelerate reaction kinetics, resulting in rapid signal generation. Additionally, the spherical DNA nanostructure, integrated with the S-CRISPR/Cas12a system, greatly enhances biostability and accelerating reaction kinetics. These features enable the platform to exhibit high sensitivity, with a limit of detection (LOD) as low as 13.75 fM, and excellent specificity, successfully distinguishing miRNA-21 from other miRNAs. The assay is also biostable, demonstrating reliable performance in complex biological samples such as human serum. This dual-acceleration approach offers a promising solution for sensitive, rapid, and specific miRNA biosensing, with potential applications in early cancer diagnosis and clinical monitoring.

INTRODUCTION

Over the past two decades, noncoding RNAs have emerged as crucial regulators involved in development, normal physiological processes, and various diseases.[1,2] Among these, microRNAs (miRNAs) stand out as a significant class of small endogenous noncoding RNAs, typically ranging from 21 to 23 nucleotides in length.[3] These molecules exert their regulatory functions by controlling gene expression at the post-transcriptional level, either through mRNA degradation or by inhibiting mRNA translation.[4] Recent expression profiling studies have highlighted the critical roles of miRNAs in a wide array of cellular processes, with their dysregulation frequently linked to various types of human malignancies[5,6] including staging, progression, prognosis, and the response to clinical therapies.[7] The early diagnosis of cancer remains one of the most formidable challenges in clinical oncology, yet it also holds the potential for significantly improving treatment outcomes.[8] The ability to predict who is at risk of developing cancer before symptoms appear could drastically alter patient management. In this context, miRNAs have garnered attention for their potential as noninvasive biomarkers, as they are detectable in the serum of cancer patients.[9,10] Their presence in serum samples presents promising prospects for developing

Received: December 31, 2024
Revised: February 3, 2025
Accepted: February 11, 2025

© XXXX American Chemical Society

https://doi.org/10.1021/acs.analchem.4c07111
Anal. Chem. XXXX, XXX, XXX−XXX

novel diagnostic tools that enable early detection, better prognostic predictions, and more precise clinical management, ultimately enhancing patient outcomes.

Traditional methods for detecting miRNAs, such as Northern blotting, fluorescence in situ hybridization (FISH), microarray analysis, and real-time quantitative PCR (qPCR), have been widely employed.[11−14] These conventional approaches have provided valuable insights into miRNA expression and function. However, they also present several limitations. For instance, Northern blotting and microarray analysis are often semiquantitative, which complicates precise measurements. FISH, while useful for localization, suffers from low sensitivity and high costs, making it less practical for widespread clinical use. Although real-time qPCR offers higher sensitivity, it is relatively complex, requiring extensive optimization and skilled personnel. These limitations highlight the pressing need for new detection methods that are not only more convenient and rapid but also highly sensitive and accessible for biomedical applications.[15,16]

Emerging technologies, particularly nonenzymatic isothermal amplification methods such as catalytic hairpin assembly (CHA)[17,18] and CRISPR/Cas12a-based assays,[19,20] have shown great promise as alternatives to traditional miRNA detection methods. CHA, in essence, is a signal amplification technique that uses two partially complementary hairpin probes and a single-stranded target initiator in a bulk solution. The target initiator hybridizes with one of the hairpin probes, triggering repeated hybridization events between the two probes. For CRISPR/Cas12a, it consists of CRISPR RNA (crRNA) and the Cas12a nuclease, which recognizes and cleaves target DNA. This cleavage activates the collateral trans-cleavage activity of Cas12a, initiating indiscriminate cleavage of single-stranded DNA reporters. The CRISPR/Cas12a system has been widely applied as powerful analytical tools for DNA and RNA targets detection in the field of biomedical analysis.[21−25] The synergy between CHA and CRISPR/Cas12a system would enhance signal amplification and improve detection accuracy, thereby increasing both sensitivity and specificity, which enables the detection of ultralow miRNA concentrations for clinical disease diagnostics.[26,27] However, traditional CHA amplifiers rely on the random diffusion of dissociative probes in bulk solution, making the probe collisions infrequent and leading to low efficiency and slow signal generation.[28,29] In the case of CRISPR/Cas12a, without a preamplification step, direct nucleic acid detection is limited to a detection threshold in the picomolar range,[30] and the trans-cleavage rate when using a single-stranded reporter is constrained.[31] Additionally, single- and double-stranded oligonucleotide probes are susceptible to nuclease degradation in biological samples, which can result in false-positive results.[32,33] Although CHA products are typically double-stranded DNA duplexes and can be coupled with CRISPR/Cas12a to improve assay sensitivity, the biostability of the integrated CHA@CRISPR/Cas12a system in complex biological samples, particularly human blood or serum, remains compromised due to the presence of nucleases.

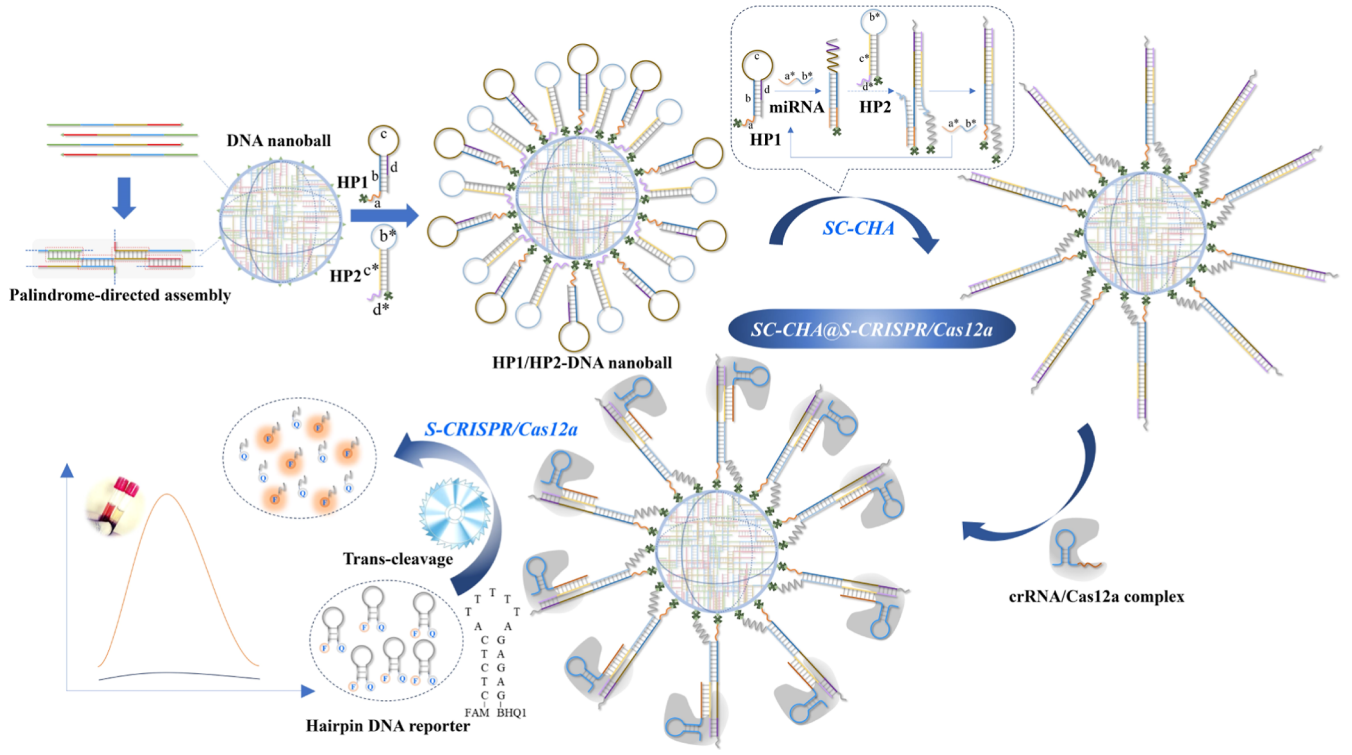
DNA nanostructures are artificially designed, self-assembled structures made from DNA molecules, with a wide range of applications including biosensing, drug delivery, and molecular computing.[34,35] Unlike single- or double-stranded DNA, DNA nanostructures feature well-ordered, rigid, multistrand architectures that often adopt complex 3D conformations.[36] This structural stability makes them less susceptible to nuclease degradation in biological fluids, enhancing their potential for use in various biological environments.[32,37] Furthermore, the higher-order structures of DNA nanostructures enable a spatial confinement effect, bringing tethered probes into close proximity, which increases their local concentration and significantly accelerates reaction kinetics.[38,39] This increased local concentration of probes enhances the efficiency of molecular interactions, leading to improved detection speed. In particular, spherical DNA nanostructures are three-dimensional assemblies of DNA strands that adopt nanoscale, spherical configurations.[40] Their dense, compact conformation grants them significantly greater resistance to enzymatic degradation compared to linear or single-stranded DNA.[41] This enhanced biostability is especially advantageous in human blood or serum, where nucleases rapidly degrade unprotected DNA. Moreover, spherical DNA nanostructures can be conveniently prepared through a one-pot assembly process using DNA strands, offering a significantly simpler and more straightforward approach compared to the synthesis of some nanoparticles, such as gold nanoparticles, which typically require complex procedures involving heating, stirring, and cooling. Based on these appealing advantages, in this study, we developed a DNA nanosensing platform, termed spatial confining CHA-activated spherical CRISPR/Cas12a system (SC-CHA@S-CRISPR/Cas12a), for the direct detection of miRNAs in human serum to address the limitations of conventional CHA, CRISPR/Cas12a, as well as traditional integrated CHA@CRISPR/Cas12a system and further enhance their performance. This platform utilizes a biotinylated palindrome-rich assembly sequence (PAS) to form DNA nanoballs through palindrome-structure-directed intermolecular reverse-reading. Two hairpin probes, termed HP1 and HP2, are biotinylated to facilitate the CHA process on the surface of the DNA nanoballs. In the absence of miRNA, HP1 and HP2 remain stable, preventing any reaction. Upon the introduction of miRNA-21, the unfolding of HP1 is triggered, which then hybridizes with HP2, releasing the miRNA and initiating a cyclic amplification process of CHA. With the spatial confinement effect of the DNA nanoball, the close proximity of HP1 and HP2 enhances local probe concentrations and reduces physical distances between them, thus accelerating reaction kinetics. The subsequent CHA products bind to crRNA and Cas12a protein, activating a S-CRISPR/Cas12a system to cleave a hairpin DNA reporter instead of the conventional single-stranded DNA reporter, further speeding up the signal generation. Additionally, the spherical DNA nanostructure enhances the biostability of the system by protecting the components from nuclease degradation in complex serum samples, enabling rapid, sensitive, and quantitative miRNA detection with significantly improved sensitivity and biostability compared to conventional detection methods.

EXPERIMENTAL SECTION

Materials and Reagents. All oligonucleotides, 20× PBS buffer (200 mM Na_2HPO_4, 35 mM KH_2PO_4, 2.74 M NaCl, 53 mM KCl, pH 7.2−7.6), 30% acryl/bis solution (29:1), 5× TBE buffer (445 mM tris, 445 mM boric acid, 10 mM EDTA, pH 8.0−8.6), DEPC-treated water, and 10,000 × 4S Red Plus were obtained from Shanghai Sangon Biological Engineering Technology and Services (Shanghai, China). The Cas12a protein was purchased from NEB England Biolabs (Beijing, China). All other chemicals used were of analytical grade and

https://doi.org/10.1021/acs.analchem.4c07111
Anal. Chem. XXXX, XXX, XXX−XXX

Scheme 1. Schematic Representation of the Detection Process and Signal Amplification of SC-CHA@S-CRISPR/Cas12a for the Detection of miRNA-21[a]



[a]The platform uses a palindrome-rich strand (PAS) to form DNA nanoballs, with hairpin probes (HP1, HP2) anchored to their surface. Target miRNA triggers catalytic hairpin assembly (CHA), accelerated by spatial confinement. HP1/HP2 complexes activate S-CRISPR/Cas12a, cleaving hairpin reporters to amplify fluorescence for sensitive miRNA detection.

were utilized without further purification. Ultrapure water, with an electrical resistance of 18.25 MΩ, was sourced from a Kerton lab MINI water purification system (UK). All oligonucleotide sequences are listed in Table S1, along with sequence analysis in the footnotes. DNA stock solutions were prepared by dissolving oligonucleotides in 1× TE buffer (10 mM tris-HCl, 1 mM EDTA, pH 8.0). RNAs were dissolved in DEPC-treated water to prepare stock solutions. The DNA annealing process was conducted using a T100 thermal cycler (Bio-Rad Laboratories, Inc., USA).

Gel Electrophoresis Characterization. A 14% non-denaturing polyacrylamide gel (native-PAGE) was used to analyze the self-assembly of DNA nanostructures, while a 2% agarose gel was used to analyze the CHA. To prepare the 14% native-PAGE, 4.9 mL dd-H_2O, 7 mL 30% acrylamide, 3 mL 5× TBE buffer, 110 μL ammonium persulfate, and 10 μL TEMED were mixed. Next, 10 μL of the DNA sample, 2 μL of 6× loading buffer, and 2 μL of 100 × 4S Red Plus nucleic acid stain were mixed at room temperature. The mixture was then loaded into the wells of the freshly prepared gel, and electrophoresis was performed at a constant voltage of 100 V for 60 min. For the preparation of the 2% agarose gel, 0.6 g of agarose was dissolved in 30 mL of 1× TBE buffer, and 3 μL of 10,000× GleRed dye was added. The solution was mixed thoroughly to prepare the gel. Subsequently, 5 μL of the DNA sample and 2 μL of 6× loading buffer were mixed at room temperature and loaded into the wells of the prestained 2% agarose gel. Electrophoresis was carried out at a constant voltage of 147 V for 25 min.

Fluorescence Measurements. Fluorescence measurements were conducted using a F97Pro Spectrofluorophotometer (Lengguang, Shanghai). The excitation wavelength was set to 490 nm, and the emission spectra were recorded from 500 to 650 nm. The peak fluorescence intensity at 521 nm was used as the key parameter to evaluate the performance of the assay in this study.

Atomic Force Microscopy (AFM) Imaging of DNA Nanoballs. Approximately 10 μL of the assembled DNA sample was deposited onto a clean mica sheet and allowed to adhere for 10 min. The mica sheet was then washed twice with 200 μL of ultrapure water to remove any excess material. Following washing, the sample was dried with nitrogen gas and subsequently heated in an oven at 37 °C for 24 h to ensure complete preparation. The mica sheet containing the prepared sample was mounted onto the sample stage of an AFM (Bruker, Germany). AFM imaging was performed using the QI mode of ScanAsyst-Air at room temperature under ambient conditions.

Real-Time Fluorescence Monitoring. The real-time fluorescence response was recorded using an isothermal amplification fluorescence detection instrument (H1600, Bio-Gener). The reaction mixture included 8 μL of 10× NEBuffer 2.1, 7 μL of DEPC-treated water, 2 μL of a 5 μM hairpin DNA reporter, 1 μL of 1 μM gRNA, 1 μL of 1 μM CRISPR/Cas12a, and 1 μL of CHA amplification products. The reaction temperature was set at 37 °C, and the recording duration was 4 h.

https://doi.org/10.1021/acs.analchem.4c07111
Anal. Chem. XXXX, XXX, XXX−XXX

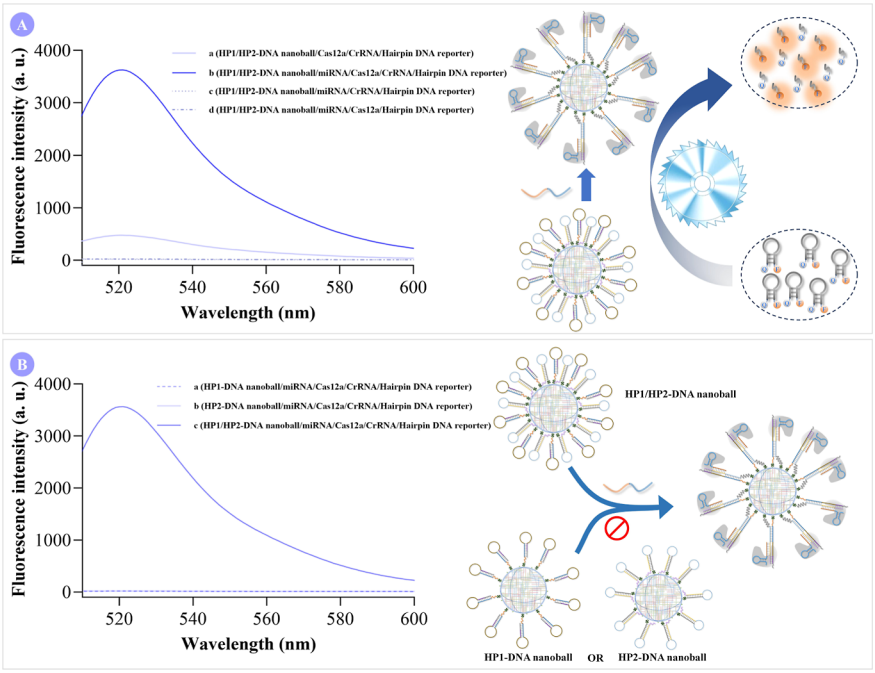


Figure 1. (A) Fluorescence signal analysis under different experimental conditions: (a) HP1/HP2−DNA nanoball + Cas12a + CrRNA + Hairpin DNA reporter; (b) HP1/HP2−DNA nanoball + miRNA + Cas12a + CrRNA + Hairpin DNA reporter; (c) HP1/HP2−DNA nanoball + miRNA + CrRNA + Hairpin DNA reporter; (d) HP1/HP2−DNA nanoball + miRNA + Cas12a + Hairpin DNA reporter. (B) Signal response analysis of the HP1−DNA nanoball (a), HP2−DNA nanoball (b), and HP1/HP2−DNA nanoball (c) mixed with target miRNA to activate with CRISPR/Cas12a, respectively. Experimental conditions: [Cas12a] = 1 μM; [CrRNA] = 1 μM; [Hairpin DNA reporter] = 5 μM; [miRNA-21] = 1 μM. The CHA reaction was performed at 37 °C for 1 h, followed by the CRISPR/Cas12a reaction, which was incubated at 37 °C for 1 h.

PREPARATION OF DNA NANOBALLS

To prepare the DNA nanoball, 1 μL of a 100 μM PAS was mixed with 83.3 μL of 1× TAE/Mg^{2+} buffer (20 mM tris, 2 mM EDTA, 12.5 mM $MgCl_2$, pH 7.4) and incubated at 90 °C for 5 min. The mixture was then allowed to cool slowly to room temperature to facilitate self-assembly through palindrome-directed intermolecular interactions.

Preparation of HP1 and HP2-Conjugated DNA Nanoball (HP1/HP2−DNA Nanoball). Before anchoring HP1 and HP2 to the surface of the DNA nanoball, both HP1 and HP2 were annealed to form a stabilized structure under the following conditions: 95 °C for 5 min, 63 °C for 30 min, 37 °C for 30 min, and 4 °C for 30 min. An equimolar amount of streptavidin (SAV) was then added to react with HP1 and HP2, and the total volume was adjusted to 100 μL with 1× PBS. The resultant mixture was incubated at room temperature for 2 h. Subsequently, 41.65 μL of the prepared DNA nanoball, 50 μL of the SAV/HP1 and SAV/HP2 mixture, and 8.35 μL of 1× PBS were combined and incubated at room temperature for an additional 2 h to yield the HP1/HP2−DNA nanoball.

SC-CHA@S-CRISPR/Cas12a Based miRNA Detection. For the miRNA screening, 4 μL of the HP1/HP2−DNA nanoball, 1 μL of miRNA at various concentrations, and 15 μL of tris buffer (20 mM tris-HCl, 140 mM NaCl, 5 mM KCl; pH 7.5) were thoroughly mixed and incubated at 37 °C for 60 min. After incubation, 1 μL of the resulting solution was taken and sequentially combined with 8 μL of 10× NE buffer 2.1, 7 μL of DEPC-treated water, 2 μL of a 5 μM hairpin DNA reporter, 1 μL of a 1 μM crRNA, and 1 μL of 1 μM CRISPR/Cas12a, followed by a further incubation at 37 °C for 60 min. The final mixture was diluted to a total volume of 100 μL using dd-H_2O and transferred to a micro cuvette for fluorescent recording. Notably, prior to use, the hairpin DNA reporter was heated at 95 °C for 5 min and then allowed to cool gradually to room temperature.

RESULTS AND DISCUSSION

Working Principle of miRNA Detection via SC-CHA@S-CRISPR/Cas12a. To fabricate the DNA sensing platform, we utilized a PAS and a pair of HPs that are partially complementary. The PAS was biotinylated at its 3′ end and contained four palindromic domains, serving as the building block for DNA nanoball assembly. Each palindromic domain should be carefully designed. If the sequence contains fewer bases, the intermolecular hybridization force may be insufficient to facilitate effective self-assembly. Conversely, an excessive number of bases could lead to intramolecular folding of individual PAS probes rather than the intended intermolecular interactions required for self-assembly. Both HPs were also biotinylated at their 3′ ends and employed to facilitate the CHA on the DNA nanoballs. As shown in Scheme 1, the assembly process begins with the palindrome-rich strand, where the well-known reverse-reading capability of palindromic structures allows each domain in one strand to hybridize with its counterpart in another, forming double-stranded DNA duplexes that promote intermolecular assembly. This self-assembly ultimately generates three-dimensional spherical DNA nanostructures, as confirmed by AFM (shown in Figure S1). Subsequently, the biotinylated HP1 and HP2 are prebound to streptavidin (SAV), anchoring them to the DNA nanoball's surface via specific SAV−biotin interactions. In the absence of the target miRNA, HP1 and HP2 remain stable as hairpin structures on the HP1−HP2/DNA nanoball, preventing any reactions. Upon introduction of the target miRNA-21, the target sequence (comprising domains a* and b*)

https://doi.org/10.1021/acs.analchem.4c07111
Anal. Chem. XXXX, XXX, XXX−XXX

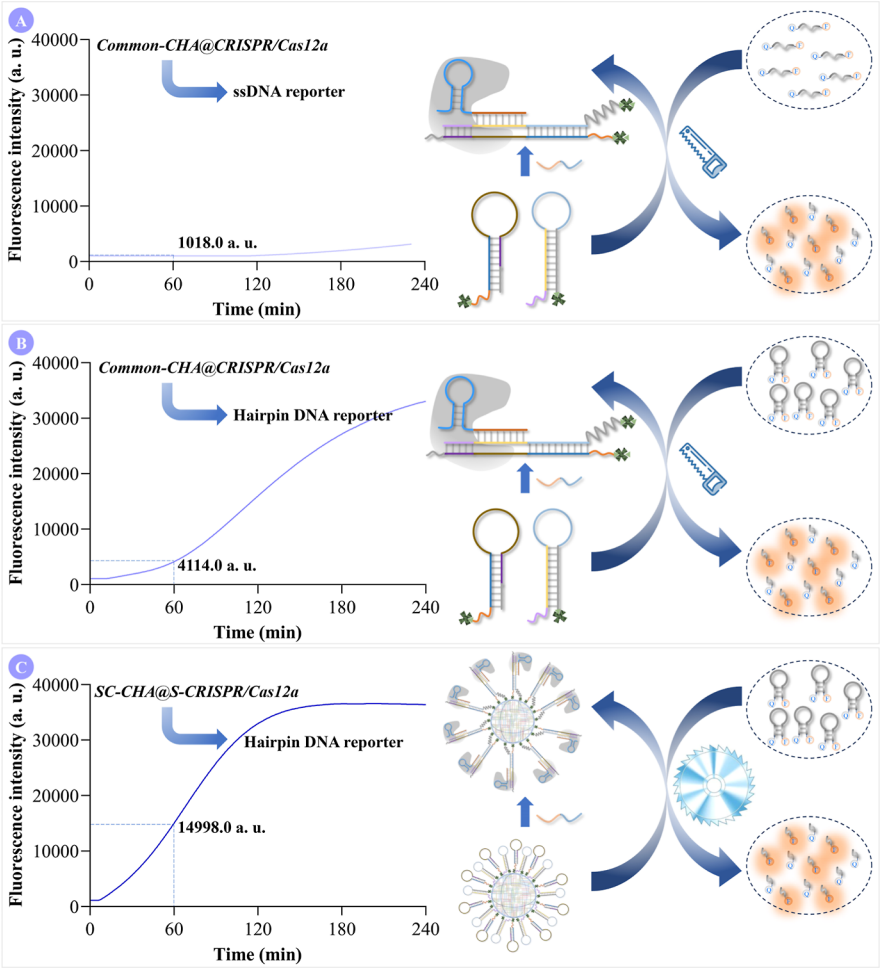


Figure 2. Real-time fluorescence response and brief illustration of different signal amplification strategies: (A) target induced common-CHA@CRISPR/Cas12a system for the cleavage of ssDNA reporter; (B) target induced common-CHA@CRISPR/Cas12a system for the cleavage of hairpin DNA reporter; (C) target induced SC-CHA@CRISPR/Cas12a system for the cleavage of hairpin DNA reporter. The target induced common-CHA@CRISPR/Cas12a system for the cleavage of ssDNA reporter exhibits the slowest fluorescence generation, showing very weak significant enhancement even about 60 min. In contrast, the incorporation of a hairpin DNA reporter probe accelerates the signal amplification, with notable enhancement observed about 60 min. The maximal enhancement in reaction kinetics is achieved with the addition of a DNA nanoball to confine HP1 and HP2 on its surface and using hairpin DNA reporters, resulting in an obvious signal increase of the SC-CHA@CRISPR/Cas12a. This demonstrates the effectiveness of hairpin reporters and spatial confinement in improving amplification kinetics. Experimental conditions: [HP1] = [HP2] = 1 μM; [Cas12a] = 1 μM; [CrRNA] = 1 μM; [Hairpin DNA reporter] = 5 μM; [ssDNA reporter] = 5 μM; [miRNA-21] = 1 μM. For the real-time fluorescence monitoring, the CHA reaction was performed at 37 °C for 1 h, followed by the CRISPR/Cas12a reaction, which was incubated at 37 °C for 4 h.

complements the toehold (domain a) and stem (domain b) regions of HP1, thereby serving as an initiator that triggers the unfolding of HP1's hairpin structure. This interaction forms the HP1/miRNA-21 complex, which has a sticky end (domains c and d) that can hybridize with the toehold (domain d*) and stem (domain c*) of HP2. This unfolding of HP2 via strand displacement releases the target miRNA and generates the HP1/HP2 complex. Since both HP1 and HP2 are tethered to the same DNA nanoball, the process is significantly accelerated due to the spatial confinement effect of this DNA nanoball reduces the physical distance between HP1 and HP2 and enhances their local concentrations. The released target miRNA re-enters the cycle, forming additional HP1/miRNA-21 complexes and HP1/HP2 complexes, achieving cyclic signal amplification. The rapid reaction kinetics lead to the swift accumulation of numerous HP1/HP2 complexes through the programmable DNA circuit. Notably, each HP1/HP2 complex contains a protospacer and a PAM sequence. They can be specifically recognized by the Cas12a/crRNA complex and lead to the formation of S-CRISPR/Cas12a system. Upon adding hairpin DNA reporter, the activated S-CRISPR/Cas12a system with collateral cleavage activity exerts rapid and nonspecific cleavage of reporters, resulting in the release of a significantly enhanced measurable fluorescence signal. Moreover, the hairpin reporter's design effectively separates single-stranded portions preferentially cleaved by activated Cas12a proteins (the loop), further resulting in a second acceleration of signal amplification. Additionally, from a signal transduction perspective, using stem-loop DNA reporters offers significant advantages over conventional short ssDNA probes, providing superior quenching efficiency and a lower fluorescence background due to the close contact between the fluorophore and quencher. Consequently, the emitted fluorescence intensity of the SC-CHA@S-CRISPR/Cas12a platform directly correlates with the initial amount of

https://doi.org/10.1021/acs.analchem.4c07111
Anal. Chem. XXXX, XXX, XXX−XXX

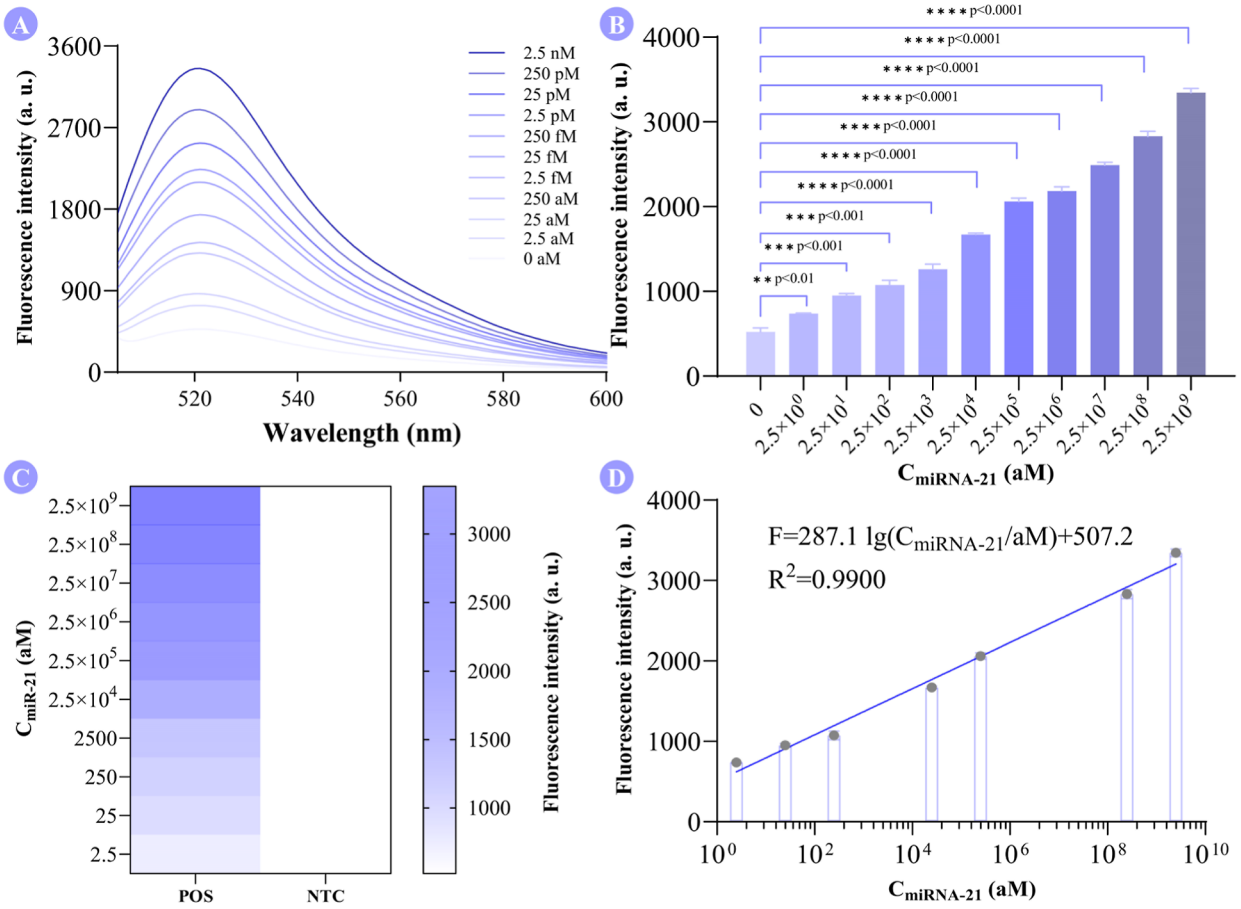


Figure 3. Sensitivity investigation of the miRNA detection system. (A) Fluorescent spectra of the SC-CHA@S-CRISPR/Cas12a system in the presence of a series of target miRNA-21 concentration (from bottom to top: 0, 2.5 aM, 25 aM, 250 aM, 2.5 fM, 25 fM, 250 fM, 2.5 pM, 25 pM, 250 pM, and 2.5 nM). (B) Peak fluorescence intensity increase with varying target miRNA concentrations, from 0 to 2.5×10^9 fM. (C) Heat map of the fluorescence intensity achieved by different concentrations of the miRNA. (D) Linear relationship between peak fluorescence intensity and logarithmic target miRNA concentration. Experimental conditions: [Cas12a] = 1 μM; [CrRNA] = 1 μM; [Hairpin DNA reporter] = 5 μM. The CHA reaction was performed at 37 °C for 1 h, followed by the CRISPR/Cas12a reaction, which was incubated at 37 °C for 1 h. Error bars are estimated from three repetitive tests.

miRNA, enabling high-speed and sensitive quantitative detection.

Feasibility Demonstration of the miRNA Detection Assay. To assess the feasibility of the miRNA detection assay, we challenged the system both in the presence and absence of target miRNA. As shown in Figure 1A, the negative control sample exhibited a negligible background signal (line a), whereas the target miRNA-positive sample induced a significantly amplified fluorescence, much higher than the control (line b). Additionally, we tested the system in the absence of Cas12a protein (line c) and crRNA (line d). As expected, no signal enhancement was observed in these cases, indicating that the CRISPR/Cas12a system could not be activated, and no DNA reporter cleavage occurred. We further evaluated whether the signal amplification was due to the SC-CHA process activating the CRISPR/Cas12a system for hairpin DNA reporter cleavage. As illustrated in Figure 1B, when the HP1−DNA nanoball was incubated with miRNA, no signal was detected (line a). Similarly, the incubation of the HP2−DNA nanoball with miRNA did not result in any observable signal enhancement. This phenomenon can be attributed to the fact that while HP1 is capable of hybridizing with miRNA to form HP1/miRNA complexes, it lacks the specific sequence required to activate the CRISPR/Cas12a system. For HP2, since there are no complementary bases to the target miRNA, the mixture of HP2 and miRNA could not activate CRISPR/Cas12a, thus unable to generate a fluorescence signal. Interestingly, when both HP1 and HP2 DNA nanoballs were introduced together with miRNA, a substantial fluorescence signal increase was observed in line c, much higher than that of line a and b. This significant signal enhancement can be attributed to the CHA process, where the target miRNA is recycled and used multiple times, leading to maximal activation of the CRISPR/Cas12a system and resulting in amplified fluorescence emission. The signal differences observed among lines a, b, and c confirm that the CHA process is indeed responsible for the activation of CRISPR/Cas12a and subsequent signal amplification in the current detection system. The characterization of the CHA by gel electrophoresis was given in Figure S2.

Validation of Dual-Accelerated Signal Amplification Effect. Following our characterization of the amplification protocol's feasibility, we performed a comparative kinetic analysis to validate the dual-accelerated signal amplification effect. As shown in Figure 2A, we tested common CHA strategies using HP1 and HP2, but without the DNA nanoball to activate CRISPR/Cas12a. The reporter used was single-stranded (ssDNA: FAM-TTATT-BHQ), which lacks a hairpin

https://doi.org/10.1021/acs.analchem.4c07111
Anal. Chem. XXXX, XXX, XXX−XXX

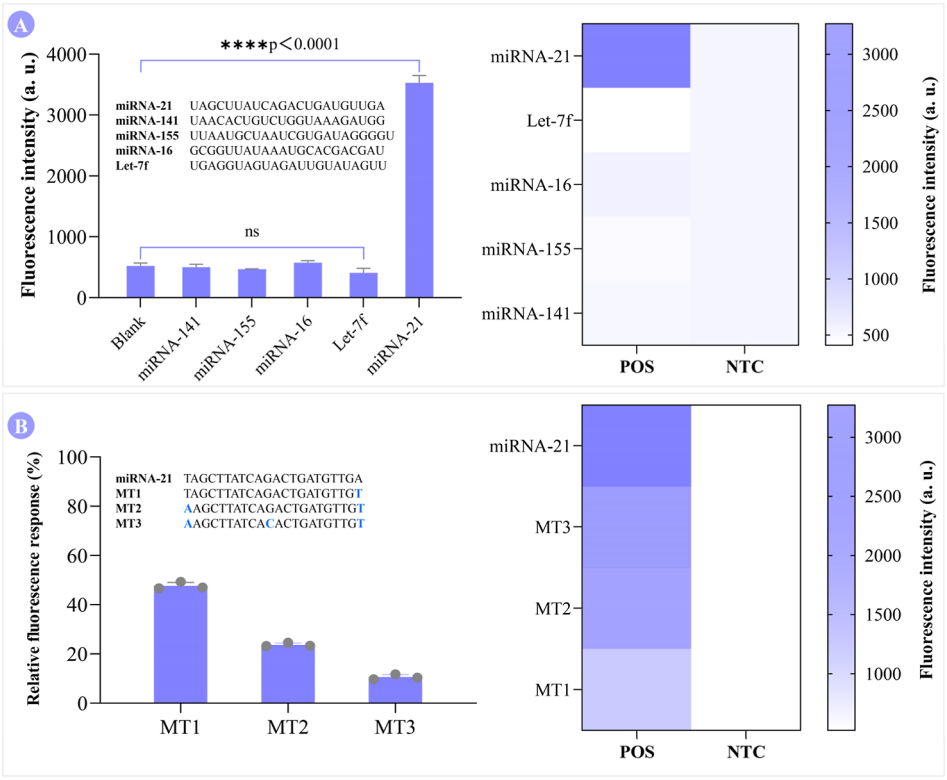


Figure 4. (A) Fluorescence signal intensities of nontarget miRNAs (miRNA-141, miRNA-155, miRNA-16, and let-7f) and target miRNA-21. (B) Fluorescence signal intensities of base mutant miRNAs (MT-1a, MT-1b, MT-2a, and MT-3a) and target miRNA-21. Only miRNA-21 induced a significant fluorescence increase, confirming the high specificity of the system in distinguishing miRNA-21 from other miRNAs. Experimental conditions: [Cas12a] = 1 μM; [CrRNA] = 1 μM; [Hairpin DNA reporter] = 5 μM; [miRNA-141] = [miRNA-155] = [miRNA-16] = [let-7f] = [MT2−1] = [MT2−2] = [MT3] = [miRNA-21] = 1 μM. The CHA reaction was performed at 37 °C for 1 h, followed by the CRISPR/Cas12a reaction, which was incubated at 37 °C for 1 h. Error bars are estimated from three repetitive tests.

structure. In this setup, only minimal signal enhancement was observed, even after 60 min (line a). This delay is likely due to random molecular collisions among the target miRNA, HP1, and HP2 in the bulk solution. In contrast, as shown in Figure 2B, substituting the common ssDNA reporter with the current hairpin DNA reporter significantly accelerated the signal amplification (line b). Within about 60 min, we observed a marked signal increase above the baseline, demonstrating the effectiveness of the hairpin DNA reporter in improving amplification kinetics than the common ssDNA reporter. Most notably, when we incorporated a DNA nanoball to confine HP1 and HP2 on its surface, facilitating SC-CHA for S-CRISPR/Cas12a activation and cleavage of the hairpin DNA reporter, we achieved maximal enhancement in reaction kinetics in Figure 2C. In this setup, a noticeable signal increase over the baseline was evident in 60 min. These results support our study that using DNA nanoarchitecture as a carrier creates a spatial confinement effect, which elevates the local concentrations of both HP1 and HP2. This, in turn, significantly enhances the molecular collision rate, further accelerating the overall reaction speed.

Sensitivity Investigation. Under optimized experimental parameters (Figure S3), we assessed the sensitivity of the SC-CHA@S-CRISPR/Cas12a amplification system by detecting the target miRNA concentration across various concentrations of 0, 2.5 aM, 25 aM, 250 aM, 2.5 fM, 25 fM, 250 fM, 2.5 pM, 25 pM, 250 pM, and 2.5 nM. The resulting detection outcomes, as illustrated in the Figure 3A, showed a clear increase in fluorescence intensity correlating with rising concentrations of the target miRNA from 2.5 aM to 2.5 nM. A linear relationship between peak fluorescence signal intensity and target miRNA concentration was established in Figure 3B, represented by the equation: $F_{521} = 287.1 \lg (C_{\text{miRNA-21}}/\text{aM}) + 507.2$ with a high correlation coefficient of ($R^2 = 0.9900$). To determine the limit of detection (LOD), we employed the IUPAC-recommended method, which relies on an experimentally determined signal-to-noise ratio (S/N). The concentration of the sample that satisfied the condition $3 < S/N < 5$ was designated as the LOD for our detection platform. According to this method, the LOD was determined to be approximately 13.75 fM. Furthermore, all fluorescence peak data exhibited relative standard deviations (RSDs) below 5.0%, demonstrating acceptable reproducibility of the system. When compared to various reported methods for miRNA detection, as summarized in Table S2, our approach demonstrates not only an enhanced detection speed but also superior sensitivity, reinforcing its potential for practical applications in miRNA diagnostics and monitoring.

Specificity Investigation. It is well-known that miRNAs comprise a vast family and exhibit significant homology. Therefore, in addition to evaluating the system's sensitivity, we aimed to assess its ability to specifically identify target miRNA-21 among other miRNAs. To evaluate specificity, we first selected nontarget analytes, including miRNA-141, miRNA-155, miRNA-16, and let-7f, as the target analytes to be tested against the target miRNA-21. As shown in Figure 4A, the fluorescence signal intensities generated by these nontarget miRNAs were comparable to the control group, which

https://doi.org/10.1021/acs.analchem.4c07111
Anal. Chem. XXXX, XXX, XXX−XXX

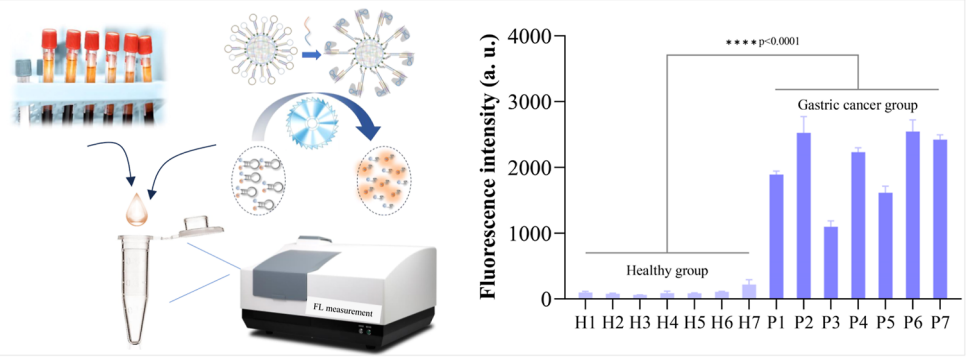


Figure 5. Real sample analysis of miRNA-21 in serum samples. Fluorescence intensity analysis of miRNA-21 in serum samples from gastric cancer patients and healthy individuals. The fluorescence intensity corresponding to miRNA-21 was significantly higher in the serum of gastric cancer patients, confirming the system's reliability for detecting miRNA-21 in complex biological samples. Experimental conditions: [Cas12a] = 1 μM; [CrRNA] = 1 μM; [Hairpin DNA reporter] = 5 μM. The CHA reaction was performed at 37 °C for 1 h, followed by the CRISPR/Cas12a reaction, which was incubated at 37 °C for 1 h. Error bars are estimated from three repetitive tests.

contained no targets. In contrast, only the presence of target miRNA-21 induced a significant enhancement in fluorescence intensity. Additionally, we assessed the ability of the SC-CHA@S-CRISPR/Cas12a system to differentiate base mutations (one-base mutation, MT1; two-base mutation, MT2; three-base mutation, MT3) from the perfectly matched target. The system's mutation detection capability was evaluated by measuring the relative fluorescence response using the formula $[(F_M - F_0)/(F_T - F_0)]$. F_M, F_T, and F_0 represent the peak fluorescent values obtained from the mutant target, the target miRNA-21, and the blank sample, respectively. As shown in Figure 4B, the results indicate a decrease in fluorescence intensity as the number of mutated bases increased. The relative responses for MT1, MT2, and MT3 were 47.61%, 23.66%, and 10.61%, respectively. This trend can be attributed to the fact that the more mutated bases present in the target analyte, the more the CHA reaction is weakened, which in turn reduces the activation of CRISPR/Cas12a for trans-cleavage of the DNA reporter. These findings demonstrate that our system is highly selective for precise miRNA detection, a crucial feature for effective diagnostic applications, and highlight its ability to accurately distinguish between closely related miRNAs.

Real Sample Analysis. Finally, to evaluate the practical applicability of our SC-CHA@S-CRISPR/Cas12a amplification system in analyzing complex real samples, we applied it to detect miRNA-21 in serum samples from patients diagnosed with gastric cancer. The demonstration of the DNA nanostructure in enhancing its biostability is provided in Figure S4. Previous studies have reported that the expression level of miRNA-21 in the circulating blood of gastric cancer patients is significantly elevated compared to that of healthy individuals.[42] In our study, we selected seven serum samples from gastric cancer patients and seven from healthy individuals to conduct a qualitative analysis using our amplification method. The detection results, presented in Figure 5, revealed that the fluorescence intensity corresponding to miRNA-21 in the serum of gastric cancer patients was markedly higher than that observed in healthy individuals. These findings align well with existing literature that documents the upregulation of miRNA-21 in gastric cancer cases, further confirming the reliability and accuracy of our system in detecting miRNA-21 from complex human biological fluids. This capability not only reveals the potential of our method for clinical applications but also highlights its significance in the early diagnosis and monitoring of gastric cancer.

CONCLUSIONS

In conclusion, we have developed a dual-accelerated signal amplification platform for miRNA detection, combining SC-CHA on DNA nanoballs with S-CRISPR/Cas12a-mediated trans-cleavage of hairpin DNA reporters. This system addresses critical challenges in miRNA detection, including sensitivity, reaction kinetics, and biostability, particularly in complex biological matrices like human serum. The DNA nanoballs not only enhance the biostability of the reaction system, but also produce a spatial confinement effect, significantly enhancing local probe concentrations to accelerate the CHA process and improving reaction kinetics for activation of S-CRISPR/Cas12a system. These advantages enable rapid and robust signal amplification. The S-CRISPR/Cas12a system efficiently cleavages hairpin DNA reporters, amplifying the fluorescence signal, which directly correlates with miRNA concentration. Our platform achieved outstanding sensitivity, specificity, and biostability, effectively distinguishing miRNA-21 from related miRNAs. Additionally, it showed resilience in complex biological samples, demonstrating its potential for real applications. Serum analysis of gastric cancer patient samples highlighted its clinical utility. This dual-accelerated approach offers a powerful, versatile solution for rapid, sensitive, and specific miRNA detection, with strong potential for early disease diagnosis. To further advance this platform, future work will focus on integrating it with portable detection devices to enable point-of-care testing, as well as exploring its adaptability for detecting other nucleic acid biomarkers, such as circulating tumor DNA or viral RNA, to expand its utility in diverse diagnostic and research contexts. Overall, our work paves the way for DNA nanostructure-based CRISPR/Cas12a sensing platforms in clinical diagnostics and research.

ASSOCIATED CONTENT

Supporting Information

The Supporting Information is available free of charge at https://pubs.acs.org/doi/10.1021/acs.analchem.4c07111.

Sequence analysis, gel electrophoresis characterization, optimization of experimental conditions, biostability investigation, oligonucleotide sequences, and methods comparison (PDF)

https://doi.org/10.1021/acs.analchem.4c07111
Anal. Chem. XXXX, XXX, XXX−XXX

AUTHOR INFORMATION

Corresponding Author

Jianguo Xu − *Jiaxing Key Laboratory of Molecular Recognition and Sensing, College of Biological and Chemical Engineering, Jiaxing University, Jiaxing 314001, China;* orcid.org/0000-0002-0187-2623; Email: jgxu0816@163.com

Authors

Zhuqi Sui − *Jiaxing Key Laboratory of Molecular Recognition and Sensing, College of Biological and Chemical Engineering, Jiaxing University, Jiaxing 314001, China*

Baoqiang Chen − *Jiaxing Key Laboratory of Molecular Recognition and Sensing, College of Biological and Chemical Engineering, Jiaxing University, Jiaxing 314001, China*

Jia Zhao − *Jiaxing Key Laboratory of Molecular Recognition and Sensing, College of Biological and Chemical Engineering, Jiaxing University, Jiaxing 314001, China; Fujian Key Laboratory of Translational Research in Cancer and Neurodegenerative Diseases, School of Basic Medical Sciences, Fujian Medical University, Fuzhou 350122, China*

Haidong Yang − *Jiaxing Key Laboratory of Molecular Recognition and Sensing, College of Biological and Chemical Engineering, Jiaxing University, Jiaxing 314001, China*

Longhua Guo − *Jiaxing Key Laboratory of Molecular Recognition and Sensing, College of Biological and Chemical Engineering, Jiaxing University, Jiaxing 314001, China;* orcid.org/0000-0003-0706-0973

Complete contact information is available at: https://pubs.acs.org/10.1021/acs.analchem.4c07111

Author Contributions

All authors have given approval to the final version of the manuscript.

Notes

The authors declare no competing financial interest.

ACKNOWLEDGMENTS

This work was financially supported by Zhejiang Provincial Natural Science Foundation of China under grant no. LZ25C200005 and Anhui Provincial Natural Science Foundation of China under grant no. 2308085MB57.

REFERENCES

(1) Nemeth, K.; Bayraktar, R.; Ferracin, M.; Calin, G. A. *Nat. Rev. Genet.* **2024**, *25* (3), 211−232.

(2) Statello, L.; Guo, C.-J.; Chen, L.-L.; Huarte, M. *Nat. Rev. Mol. Cell Biol.* **2021**, *22* (2), 96−118.

(3) Garcia-Martin, R.; Wang, G.; Brandão, B. B.; Zanotto, T. M.; Shah, S.; Kumar Patel, S.; Schilling, B.; Kahn, C. R. *Nature* **2022**, *601* (7893), 446−451.

(4) Shang, R.; Lee, S.; Senavirathne, G.; Lai, E. C. *Nat. Rev. Genet.* **2023**, *24* (12), 816−833.

(5) Kong, Y. W.; Ferland-McCollough, D.; Jackson, T. J.; Bushell, M. *Lancet Oncol.* **2012**, *13* (6), e249−e258.

(6) Yu, F.; Wang, Y.; Yu, C.; Zhang, W.; Bai, X. *J. Anal. Test.* **2024**, *8* (2), 237−244.

(7) Diener, C.; Keller, A.; Meese, E. *Trends Genet.* **2022**, *38* (6), 613−626.

(8) Crosby, D.; Bhatia, S.; Brindle, K. M.; Coussens, L. M.; Dive, C.; Emberton, M.; Esener, S.; Fitzgerald, R. C.; Gambhir, S. S.; Kuhn, P.; et al. *Science* **2022**, *375* (6586), No. eaay9040.

(9) Cai, S.; Pataillot-Meakin, T.; Shibakawa, A.; Ren, R.; Bevan, C. L.; Ladame, S.; Ivanov, A. P.; Edel, J. B. *Nat. Commun.* **2021**, *12* (1), 3515.

(10) Sohel, M. M. H. *Life Sci.* **2020**, *248*, 117473.

(11) Peng, H.; Newbigging, A. M.; Reid, M. S.; Uppal, J. S.; Xu, J.; Zhang, H.; Le, X. C. *Anal. Chem.* **2020**, *92* (1), 292−308.

(12) Jet, T.; Gines, G.; Rondelez, Y.; Taly, V. *Chem. Soc. Rev.* **2021**, *50* (6), 4141−4161.

(13) Wang, Q.; Xia, J.; Yang, C.; Chen, X.; Chen, B.; Li, Y.; Huang, H.; Lin, B.; Guo, L.; Xu, J. *Anal. Chem.* **2024**, *96* (35), 14205−14214.

(14) Wang, Q.; Zhou, T.; Xue, D.; Yang, H.; Sui, Z.; Yuan, X.; Xu, J. *Chem. Commun.* **2024**, *60* (21), 2910−2913.

(15) Wang, J.; Sun, J.; Zhang, J.; Shen, C.; Zhang, X.; Xu, J. *Anal. Chem.* **2022**, *94* (10), 4437−4445.

(16) Zeng, Y.; Yue, H.; Cao, B.; Li, Y.; Yang, M.; Mao, C. *Angew. Chem., Int. Ed.* **2022**, *61* (45), No. e202210121.

(17) Luo, Z.; Li, Y.; Zhang, P.; He, L.; Feng, Y.; Feng, Y.; Qian, C.; Tian, Y.; Duan, Y. *TrAC, Trends Anal. Chem.* **2022**, *151*, 116582.

(18) Miao, P. *Anal. Chem.* **2023**, *95* (17), 6760−6764.

(19) Hu, M.; Qiu, Z.; Bi, Z.; Tian, T.; Jiang, Y.; Zhou, X. *Proc. Natl. Acad. Sci. U. S. A.* **2022**, *119* (26), No. e2202034119.

(20) Yuan, A.; Sha, R.; Xie, W.; Qu, G.; Zhang, H.; Wang, H.; Le, X. C.; Jiang, G.; Peng, H. *J. Am. Chem. Soc.* **2024**, *146* (39), 26657−26666.

(21) Luo, X.; Xue, Y.; Ju, E.; Tao, Y.; Li, M.; Zhou, L.; Yang, C.; Zhou, J.; Wang, J. *Anal. Chim. Acta* **2022**, *1192*, 339336.

(22) Tao, Y.; Yi, K.; Wang, H.; Kim, H.-W.; Li, K.; Zhu, X.; Li, M. *J. Colloid Interface Sci.* **2022**, *613*, 406−414.

(23) Tao, Y.; Yi, K.; Wang, H.; Li, K.; Li, M. *Sens. Actuators, B* **2022**, *361*, 131711.

(24) Tao, Y.; Wang, H.; Ju, E.; Lao, Y.-H.; Zhang, Y.; Li, M. *Talanta* **2025**, *283*, 127153.

(25) Kong, H.; Yi, K.; Mintz, R. L.; Wang, B.; Xu, Y.; Lao, Y.-H.; Tao, Y.; Li, M. *Chem. Commun.* **2024**, *60* (17), 2301−2319.

(26) Li, X.; Yang, F.; Gan, C.; Yuan, R.; Xiang, Y. *Biosens. Bioelectron.* **2022**, *197*, 113809.

(27) Peng, S.; Tan, Z.; Chen, S.; Lei, C.; Nie, Z. *Chem. Sci.* **2020**, *11* (28), 7362−7368.

(28) Qing, Z.; Hu, J.; Xu, J.; Zou, Z.; Lei, Y.; Qing, T.; Yang, R. *Chem. Sci.* **2020**, *11* (7), 1985−1990.

(29) Xu, H.; Zheng, Y.; Chen, D.; Cheng, Y.; Fang, X.; Zhong, C.; Huang, X.; Huang, Q.; Xu, J.; Xu, J.; et al. *Anal. Chem.* **2022**, *95* (2), 1210−1218.

(30) Xu, L.; Liu, S.; Huang, Z.; Pei, X.; Li, S.; He, Y.; Tong, Y.; Liu, G. *J. Anal. Test.* **2024**, 1−7.

(31) Rossetti, M.; Merlo, R.; Bagheri, N.; Moscone, D.; Valenti, A.; Saha, A.; Arantes, P. R.; Ippodrino, R.; Ricci, F.; Treglia, I.; et al. *Nucleic Acids Res.* **2022**, *50* (14), 8377−8391.

(32) Chandrasekaran, A. R. *Nat. Rev. Chem.* **2021**, *5* (4), 225−239.

(33) Zhang, H.; Vandesompele, J.; Braeckmans, K.; De Smedt, S. C.; Remaut, K. *Chem. Soc. Rev.* **2024**, *53*, 317−360.

(34) Wang, J.; Li, Z.; Willner, I. *Angew. Chem.* **2023**, *135* (18), No. e202215332.

(35) Zhang, P.; Ouyang, Y.; Zhuo, Y.; Chai, Y.; Yuan, R. *Anal. Chem.* **2023**, *95* (1), 407−419.

(36) Rossi-Gendron, C.; El Fakih, F.; Bourdon, L.; Nakazawa, K.; Finkel, J.; Triomphe, N.; Chocron, L.; Endo, M.; Sugiyama, H.; Bellot, G.; et al. *Nat. Nanotechnol.* **2023**, *18* (11), 1311−1318.

(37) Kyriazi, M.-E.; El-Sagheer, A. H.; Medintz, I. L.; Brown, T.; Kanaras, A. G. *Bioconjugate Chem.* **2022**, *33* (1), 219−225.

(38) Wang, Q.; Chen, B.; Zheng, D.; Xia, J.; Wu, L.; Xu, J. *Anal. Chem.* **2023**, *95* (36), 13708−13715.

(39) Wang, Y.; Cao, L. P.; Shuai, X. J.; Liu, L.; Huang, C. Z.; Li, C. M. J. A. C. *Anal. Chem.* **2024**, *96* (11), 4597−4604.

(40) Cutler, J. I.; Auyeung, E.; Mirkin, C. A. *J. Am. Chem. Soc.* **2012**, *134* (3), 1376−1391.

(41) Mokhtarzadeh, A.; Vahidnezhad, H.; Youssefian, L.; Mosafer, J.; Baradaran, B.; Uitto, J. *Trends Mol. Med.* **2019**, *25* (12), 1066−1079.

(42) Farasati Far, B.; Vakili, K.; Fathi, M.; Yaghoobpoor, S.; Bhia, M.; Naimi-Jamal, M. R. *Life Sci.* **2023**, *316*, 121340.

https://doi.org/10.1021/acs.analchem.4c07111
Anal. Chem. XXXX, XXX, XXX−XXX